Chapter 6, pp. 153-190 of Dynamic Failure of Materials and Structures, Editors Arun Shukla, Guruswami Ravichandran, Y. Rajapakse, Springer, 2010. DOI 10.1007/978-1-4419-0446-1.

Shock Loading and Failure of Fluid-Filled Tubular Structures

Joseph E. Shepherd and Kazuaki Inaba

Abstract We consider the response of fluid-filled tubes to internal shock waves and explosions. The emphasis is on the fluid-solid coupling aspects. The coupling of axial wave propagation in the fluid to flexural waves in the tube may be characterized by a single parameter that depends only on the tube and fluid material properties and dimensions. Using this parameter as a figure of merit, we discuss the limiting cases of weak and strong coupling between the fluid wave motion and tube structural motion. Examples discussed include detonation and shock waves in gas and liquid-filled tubes of metal, polymers, and composites. The results of experiments on elastic and plastic deformation are presented as well as selected results on fracture and rupture. Detonation in gas-filled tubes usually falls in the weak coupling regime except for very thin tubes or cases of deformation that lead to tube rupture. Impact generated axial waves in liquid-filled tubes can range from weak-to-strong coupling cases depending on the tube wall thickness and material. These cases include the well-known phenomenon of water hammer and we describe the relationship of impact studies to previous work on wave-propagation in water-filled pipes.

1 Introduction

Dynamic loading of fluid-filled tubes is a situation that is encountered in industrial hazard analysis and studied in the laboratory as a model fluid-solid coupling problem. Propagating explosions or shock waves can occur inside piping systems con-

Joseph E. Shepherd
California Institute of Technology, Pasadena, CA USA 91125 e-mail: joseph.e.shepherd@caltech.edu

Kuzuaki Inaba
Tokyo Institute of Technology2-12-1 Ookayama, Meguro-ku, Tokyo, 152-8550, JAPAN e-mail: inaba@mech.titech.ac.jp

taining explosive gases and laboratory combustion facilities (Shepherd, 2009). A common situation is piping filled with water or steam and dynamic loading created by valve actuation - this is the known as “water hammer”, a well-known problem in power and process plants (Wylie and Streeter, 1993, Watters, 1984). Gas-filled and liquid-filled pipes represent extreme situations from the viewpoint of fluid-solid coupling. Gas-filled pipes represent the case of weak or one-way coupling with gas motion forcing the structural response of the pipe but relatively little or no gas motion is caused by the piping structural deformation. There is an extensive discussion of this case in Shepherd (2009) and a few representative cases are presented in this review to illustrate the features of the weak coupling case. Liquid-filled thin-wall tubes represent the case of strong or two-way coupling in which the fluid motion and structural response of the pipe must be treated simultaneously. We focus almost exclusively on the strong coupling case in the present review.

One motivation for experiments on fluid-filled tubes is the study of fluid-structure interaction in a regime that is relevant to underwater explosions. In our laboratory, we have being doing this through variations on the experiment shown in Fig. 1. A metal projectile impacts on the surface of water filling a thin-wall tube. The projectile impact creates a coupled stress wave propagating in the tube and water, as well as a reflected stress wave in the impactor. Subsequent reverberations of the stress wave in the impactor and expansions transmitted into the water results in a sharp stress wave front followed by a rapid (exponential) decay of pressure behind the front (Skews et al., 2004, Deshpande et al., 2006, Espinosa et al., 2006). Experiments using piston impact on a water-filled tube have been used extensively in studying the tensile strength of water (Trevena, 1987), metal forming of solids (Kosing and Skews, 1998, Skews et al., 2004), and as an underwater shock simulator (see the extensive review in Chap. 2 of Kedrinsky, 2005), most recently by Deshpande et al. (2006), Espinosa et al. (2006). However, in our studies we have focused on the dynamics of the tube deformation itself as a method of exploring fluid-structure interactions.

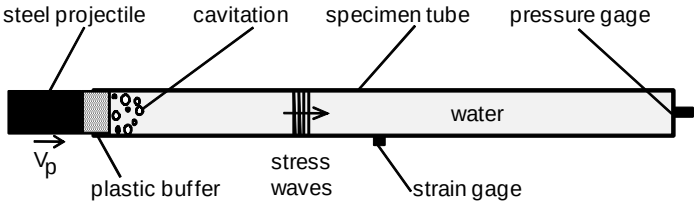

Fig. 1 Stress wave generation by piston impact on fluid inside a tube.

In this review, we report on the results of dynamics experiments of the type shown in Fig. 1 with different tubing materials, thicknesses, and various loading amplitudes. We begin by presenting the simplest theory of waves in fluid-filled tubes and use this to identify a fluid-solid coupling parameter. Following this, we describe

more sophisticated models and the regimes corresponding to the various values of the coupling parameter. Experimental results are presented for a number of different cases in each of the regimes.

2 Korteweg Model of Wave Propagation

Classical water hammer theory (Skalak, 1956, Tijsseling, 1996, Wiggert and Tijsseling, 2001) considers the coupling of the motion of an elastic pipe or tube with acoustic waves propagating in the water within the pipe. Various levels of theoretical treatment are possible (see Junger and Feit, 1986, Howe, 1998, for the foundations of fluid-structure interaction) but the key physical effects can be predicted by the very simple model proposed by Korteweg (1878) and confirmed experimentally by Joukowsky (1900) (see the historical review in Tijsseling, 1996) in which the pressures generated by the acoustic waves in the water are balanced by static stress in the surrounding pipe, considering purely elastic radial deflection uncoupled from the longitudinal motion.

The Korteweg model reproduces the essential features of classical water hammer experiments with minimal assumptions. The fluid in the tube is compressible with a density ρ_f and sound speed a_f, and the motions in the fluid are treated as quasi-one dimensional. The equations of motion of the fluid (Lighthill, 1978) are continuity (mass conservation)

$$\frac{\partial}{\partial t}(\rho A)+\frac{\partial}{\partial x}(\rho \mathrm{u} A)=0\,, \tag{1}$$

$$\rho\frac{\partial \mathrm{u}}{\partial t}+\rho \mathrm{u}\frac{\partial \mathrm{u}}{\partial x}=-\frac{\partial P}{\partial x}\,, \tag{2}$$

where ρ is the fluid density, u is the fluid velocity, A is the cross-sectional area of the tube, and P is the pressure. For small amplitude motions, we can consider pressure and density to be only slightly different from the at-rest values,

$$P'=P-P_o \ll P_o\,, \tag{3}$$

$$\rho'=\rho-\rho_o \ll \rho_o\,. \tag{4}$$

The tube area changes are relatively small,

$$A'=A-A_o \ll A_o\,, \tag{5}$$

and the velocity u is of the same order as these perturbations. Assuming isentropic motion, the pressure and density perturbations are related by

$$P'=a_f^2\rho'\,, \tag{6}$$

where the sound speed for the fluid is

$$a_f^2 = \left(\frac{\partial P}{\partial \rho}\right)_s . \tag{7}$$

Expanding the equations of motion (1 and 2), we obtain the pair of linear equations,

$$\frac{\partial}{\partial t}(\rho A) + \rho_o A_o \frac{\partial \mathrm{u}}{\partial x} = 0 , \tag{8}$$

$$\rho_o \frac{\partial \mathrm{u}}{\partial t} = -\frac{\partial P'}{\partial x} . \tag{9}$$

Cross-differentiating w.r.t. time and distance, and eliminating velocity, we can write this as

$$\frac{\partial^2 P'}{\partial x^2} = \frac{1}{A_o}\frac{\partial^2}{\partial t^2}(\rho A) . \tag{10}$$

In order to complete the model, the tube area must be determined as function of space and time $A(x,t)$. In general, this requires considering the dynamics of the motion of the tube (Skalak, 1956). The Korteweg approximation is to neglect the inertia and bending stiffness of the tube wall and only consider a force balance in the hoop (θ) direction

$$\sigma_\theta = \frac{R}{h} P' , \tag{11}$$

where σ_θ is the hoop stress, h is the wall thickness, and R is the mean tube radius. In general, the hoop stress will be a function of all components of the strain in the tube wall and depend on the radial location. However, if we use the simple membrane model of hoop stress for a cylinder and neglect longitudinal contributions, the hoop strain and stress will be related by

$$\varepsilon_\theta = \frac{\sigma_\theta}{E} , \tag{12}$$

where E is the Young's modulus of the tube wall material and the hoop strain can be computed from the change in mean radius as

$$\varepsilon_\theta = \frac{R'}{R_o} , \tag{13}$$

$$= \frac{1}{2}\frac{A'}{A_o} . \tag{14}$$

The pressure and area changes are then uniquely related

$$A' = A_o \frac{2R}{h} \frac{P'}{E} \,. \tag{15}$$

A generalization of this idea is to take the area of the tube as a function of pressure perturbation only, then

$$A = A(P') \,, \tag{16}$$

and we can write the perturbation equation (10) as a linear wave equation with a wave speed that depends both on the fluid compressibility and tube extensibility.

Korteweg equation:

$$\frac{\partial^2 P'}{\partial x^2} = \frac{1}{c^2} \frac{\partial^2 P'}{\partial t^2} \,. \tag{17}$$

Wave speed:

$$c^{-2} = \frac{1}{A_o} \frac{\partial}{\partial P'} (\rho A) \,, \tag{18}$$

$$= \frac{\partial \rho}{\partial P'} + \frac{\rho}{A_o} \frac{\partial A}{\partial P'} \,. \tag{19}$$

The first term in (19) represents the response of the fluid to pressure changes and can be interpreted in terms of the fluid sound speed (7) and the second term represents the response of the tube to pressure changes. Using the simple model of a static hoop stress balance (15), we obtain the classical formula for wave speed in elastic pipes,

$$c^{-2} = a_f^{-2} + \rho_o \frac{2R}{Eh} \,, \tag{20}$$

which was first derived by Korteweg in 1878. The coupling between the tube and fluid can be more clearly seen by writing the wave speed as

$$c = a_f \left[1 + \left(\frac{a_f^2}{a_s^2} \right) \left(\frac{\rho_f}{\rho_s} \right) \left(\frac{2R}{h} \right) \right]^{-1/2} \,, \tag{21}$$

where the bar sound speed (Kolsky, 1963) for the tube material is

$$a_s = \sqrt{\frac{E}{\rho_s}} \,, \tag{22}$$

and ρ_s is the density of the solid making up the tube. The speed of sound in the fluid a_f is often expressed in terms of the fluid bulk modulus K_f,

$$K_f = -\upsilon \left(\frac{\partial P}{\partial \upsilon} \right)_s , \qquad a_f = \sqrt{\frac{K_f}{\rho_f}} . \tag{23}$$

The wave equation (17) is an approximation to the governing equations for the motion of a fluid-filled, thin-wall tube. More general considerations (Skalak, 1956, Fuller and Fahy, 1982, Pinnington, 1997) with fewer approximations result in a coupled system of fourth-order equations for radial and longitudinal motion of the tube considered as a shell and acoustic oscillations in the fluid, discussed in the next section. There are four types of axisymmetric modes: a longitudinal motion in the shell, a coupled radial-acoustic motion (Korteweg waves) that correspond to (17), and two shell bending modes. The individual modes of shell oscillation and acoustic motion in the fluid are transformed in a set of coupled modes (Del Grosso, 1971, Sinha et al., 1992, Lafleur and Shields, 1995), the precise nature of these depends on the extent of fluid-solid coupling as discussed below. Only one of these modes, the Korteweg waves, is described by the present model (17). Properties relevant to the evaluation of the fluid-solid coupling are given in Table 1. The three terms identified

Table 1 Properties relevant to fluid-structure interaction for some representative materials.

Solids			
material	E (GPa)	ρ_s (kg·m^{-3})	a_s (m/s)
steel	200	7.8×10^3	5000
aluminum	69	2.7×10^3	5100
PMMA	3.3	1.2×10^3	*
Polycarbonate	2.6	1.25×10^3	*
glass	96	2.6×10^3	6080
GFRP	5–80	$1.4\text{-}2.2\times10^3$	*
CFRP	5–400	1.5×10^3	*
Fluids			
material	K_f (GPa)	ρ_f (kg·m^{-3})	a_f (m/s)
water	2.2	1.0×10^3	1482
mercury	28.2	13.45×10^3	1450
air	0.14 MPa	1.2	343

* Polymers are viscoelastic and composites are highly anisotropic so that there is no single well-defined bar speed for these cases.

in (21) are nondimensional ratios that form a single non-dimensional parameter β that determines the extent of fluid-solid coupling in this geometry. This parameter has been termed the "fluid loading" by Pinnington (1997) and the value plays a central role in the study of acoustic waves (Fuller and Fahy, 1982, Sinha et al., 1992) in fluid-filled tubes.

Korteweg wave speed:

$$c = \frac{a_f}{\sqrt{1+\beta}} \, .$$

The contributions to the coupling parameter

$$\beta = \underbrace{\left(\frac{a_f^2}{a_s^2}\right)}_{I} \underbrace{\left(\frac{\rho_f}{\rho_s}\right)}_{II} \underbrace{\left(\frac{2R}{h}\right)}_{III} ,$$

are:

$$I: \quad \text{longitudinal sound speed ratio ,} \tag{24}$$

$$II: \quad \text{density ratio ,} \tag{25}$$

$$III: \quad \text{geometric factor .} \tag{26}$$

Note that unlike the classical problem, treated by Taylor (1941) and Kennard (1944), of underwater shock waves reflecting from deforming plates (the original studies are given by the wartime reports in ONR 1950 and are described by Cole 1965, see also the discussions in Xue and Hutchinson, 2004, Rajendran and Narasimhan, 2006), this parameter does not include the characteristic unloading time of the load, i.e., decay time of the blast wave. Although the parameter β does indeed play the key role in determining the primary wave speed, we know from previous work (Beltman et al., 1999, Beltman and Shepherd, 2002, Chao and Shepherd, 2005b,a) on shock and detonation waves that other factors are relevant to determining the peak tube deformation. For example, nondimensional parameters that we will need to consider include:

1. ratio of unloading time to the hoop period of the tube radial oscillations;
2. ratio of the shock or detonation front speed to the group velocity of flexural waves;
3. ratio of peak induced stress to the yield stress in the solid;

For now, we will set consideration of these factors aside and just examine the role of β in fluid-structure interaction. The size of the ratios making up β can be readily computed using the properties of some representative tube materials and fluids given in Table 1. The results are given in Table 2 for two cases: 1) thin-wall tubes typical of most of our laboratory experiments so far; 2) thick-wall tubes that have been used

in a few of our tests. We have considered three fluids and four materials although it is not necessary to compute all combinations to appreciate the range of fluid-solid coupling that will exist. The theory is valid only in the limit that the tube can be treated as a shell so that the values computed for the thick-tube case are not expected to be accurate and are only given to indicate the range of fluid-solid coupling that we could anticipate in these cases. As expected, we observe that fluid-solid coupling is maximized for the thin tubes with stiff fluids and minimized for thick-tubes with highly compressible fluids. The case of air within any of the tubes is representative of the case of internal shock or detonation loading (Shepherd, 2009) and is clearly weakly coupled so that the Korteweg waves travel at the gas sound speed for small amplitude waves. For large amplitudes, the Korteweg waves travel with the shock or detonation velocity as discussed in Shepherd (2009).

Table 2 Fluid-solid coupling parameters and Korteweg wave speed for representative thick and thin wall cases.

Combination	β	Wave speed (m/s)
Thin tube, h = 0.89 mm, *D = 38.5* mm		
water-steel	0.48	1220
water-glass	0.99	1050
water-aluminum	1.4	961
water-PMMA	29.	271
mercury-steel	6.1	544
mercury-aluminum	17	335
mercury-PMMA	370	75
air-steel	3.0×10^{-5}	343
Thick tube, h = 25 mm, *D = 100* mm		
water-steel	0.044	1450
water-glass	0.092	1418
water-aluminum	0.13	1396
water-PMMA	2.7	774
mercury-steel	0.56	1159
mercury-aluminum	1.6	893
mercury-PMMA	34	244
air-steel	2.8×10^{-6}	343

3 Limiting Cases of FSI

There are some obvious limiting cases that lead to simplifications when there are extreme values of the coupling parameter β which can be rewritten as

$$\beta = \frac{\rho_f a_f^2}{\rho_s a_s^2} \times \frac{2R}{h} = \frac{K_f}{E} \times \frac{2R}{h} \, .$$

3.1 Thick, stiff tube $\beta \ll 1$

If the tube wall is sufficiently thick and/or stiff,

$$\rho_s a_s^2 h \gg 2R\rho_f a_f^2 \, ,$$

then motion of the tube wall does not influence the wave propagation speed which is just the value of the sound speed a_f in the fluid for weak waves or the wave front (shock or detonation) speed U for large amplitude waves.

Wave speed for $\beta \ll 1$:
Weak waves,

$$c \approx a_f \, .$$

Shock or detonation waves,

$$c = \mathrm{U} \, .$$

In this regime, the motion of the fluid can be computed as though the tube is rigid and the motion of the tube estimated by applying the computed pressures within the fluid as boundary conditions to the solid. This is the situation of a shock wave in air or gaseous detonation inside a metal tube, see the discussions in Beltman and Shepherd (2002), Beltman et al. (1999). As long as the tube thickness to diameter ratio exceeds 10^{-2}, i.e., wall thickness is at least 1% of the diameter, then the parameter $\beta \leq 10^{-2}$. This is satisfied for all commercial pipe and tubing components. It is possible to consider the tube to be rigid for the purposes of computing the shock or detonation wave motion allowing very simplified (one-dimensional) models of the pressure waves in the gas to be employed (Beltman and Shepherd, 2002, Beltman et al., 1999). In these cases, the deformations of the tube are usually confined to the elastic regime and the failure mode is due to cracks initiating at flaws in the tube wall, see Chao and Shepherd (2005a, 2004). It is also possible to obtain plastic deformation for extremely thin-walled, low-strength tubes and high detonation pressures (Shepherd, 2009). Fluid-structure coupling could be significant for these cases and this is a subject of active investigation in our laboratory.

If we approximate the structural dynamics of the tube as a thin shell (Tang, 1965), the motion of the shell is forced by the difference in pressure $\Delta P(x,t)$ between the interior and exterior of the tube but otherwise the fluid and solid motions are uncoupled (see the discussion in Beltman and Shepherd, 2002).

Shell model:

$$\frac{\partial N_{xx}}{\partial x} = \rho h \frac{\partial^2 u}{\partial t^2} \, , \qquad \frac{\partial M_{xx}}{\partial x} - Q_x = \rho h^3 \frac{\partial^2 \psi}{\partial t^2} \, ,$$

$$\frac{\partial Q_x}{\partial x} - \frac{N_{\theta\theta}}{R} + \Delta P = \rho h \frac{\partial^2 w}{\partial t^2} \, . \tag{27}$$

For elastic motions, the stress resultants N_{xx}, $N_{\theta\theta}$, M_{xx} and Q_x are defined as:

$$N_{xx} = \frac{Eh}{1-\nu^2}\left[\frac{\partial u}{\partial x} + \nu \frac{w}{R}\right] \, , \qquad M_{xx} = \frac{Eh^3}{12\,(1-\nu^2)} \frac{\partial \psi}{\partial x} \, ,$$

$$N_{\theta\theta} = \frac{Eh}{1-\nu^2}\left[\nu \frac{\partial u}{\partial x} + \frac{w}{R} \, ,\right] \, , \qquad Q_x = \kappa G h \left[\psi + \frac{\partial w}{\partial x}\right] \, , \tag{28}$$

where u is the axial displacement, w is the radial displacement, R is the mean shell radius, h is the shell thickness, t refers to time, ρ is the density of the shell material, ν is Poisson's ratio, E is Young's modulus, ΔP is the difference between the internal and external pressure, ψ is the rotation and κ is the shear correction factor. This particular model was used by Tang (1965) and includes terms that model the effects of shear deformation and rotary inertia. Many other versions of shell models are available and with various approximations, have been applied to fluid-structure interaction.

Obtaining the thick-wall limit with a liquid-filled tube requires a substantially stiffer and thicker-walled confining tube than for gas-filled tubes. For example, with water inside a steel tube, the simple theory predicts that the required ratio of thickness to diameter should be one, i.e., wall thickness equal to the diameter, for the parameter $\beta \leq 10^{-2}$. The approximations of a thin-wall tube is clearly no longer valid for these values and more realistic elastic models of the tube wall are required. This limit is not reached for standard sizes of commercial pipes and therefore the tube-wall motion is significant in determining the wave propagation. This situation is typical of water hammer problems and it is well known even from the earliest studies of Korteweg and Joukowsky that it is essential to include tube elasticity.

If we neglect the effects of axial stress, bending or rotary inertia and assume that the shell can be treated as a membrane, then the motion is purely radial motion if the loading is axisymmetric. The equation of motion will be

$$\rho h \frac{\partial^2 w}{\partial t^2} + \frac{N_{\theta\theta}}{R} = \Delta P(t) \, . \tag{29}$$

For elastic motions, the stress resultant is

$$N_{\theta\theta} = \frac{Eh}{1-\nu^2}\frac{w}{R}\,, \tag{30}$$

and the equation of motion is that of a forced simple harmonic oscillator, which is referred to as a single-degree-of-freedom model in the structural response community. The natural frequency of oscillation is given by the fundamental mode of radial or "hoop" motion.

Single degree of freedom model:

$$\frac{\partial^2 w}{\partial t^2} + \omega_h^2 w = \frac{\Delta P(t)}{\rho h}\,. \tag{31}$$

Natural frequency:

$$\omega_h = \frac{1}{R}\sqrt{\frac{E}{\rho(1-\nu^2)}}\,, \qquad f_h = \frac{\omega_h}{2\pi}\,. \tag{32}$$

The single degree of freedom model is quite limited since the neglect of bending stresses effectively makes each shell element independent. Including bending while still neglecting transverse shear and rotary inertia leads to the following model equation (Bhuta, 1963, Simkins, 1995), which is equivalent to that of an Euler-Bernoulli beam on an elastic foundation with a traveling load, a model that has been extensively studied in many different contexts such as the loading created by the motion of trains or rocket sleds (Kenney, 1954).

Simplified flexural wave model:

$$\frac{Eh^2}{12\rho(1-\nu^2)}\frac{\partial^4 w}{\partial x^4} + \frac{\partial^2 w}{\partial t^2} + \omega_o^2 w = \frac{\Delta P(x,t)}{\rho h}\,, \tag{33}$$

where the frequency ω_o is

$$\omega_o = \frac{1}{R}\sqrt{\frac{E}{\rho}}\,. \tag{34}$$

Steady traveling wave solutions on a long tube (Bhuta, 1963, Simkins, 1995) show a resonance when the traveling load moves at a critical propagation speed

$$V_c = \sqrt{\frac{Eh}{\rho R\sqrt{3(1-\nu^2)}}}\,. \tag{35}$$

This resonance has been observed in diverse traveling load situations such as gun tubes (Simkins et al., 1993), shock waves (Beltman et al., 1999), and detonation waves (Beltman and Shepherd, 2002). Although quite simplified, the essential features of dispersive waves and a critical speed are captured by this model.

3.2 Coupled fluid motion and tube deformation, $\beta = O(1)$

In the coupled situation, the fluid motion must be simultaneously considered with the motion of the tube. The motions are coupled together at the boundary between the tube material (solid) and the fluid inside the tube. For realistic fluids, this means that the fluid sticks to the boundary, and as long as the tube is intact, does not penetrate the boundary.[1] In addition, the tangential (shear) and normal stresses at the boundary must be continuous so that the traction forces on the boundary of the solid are equal to the surface forces obtained by evaluating the fluid stress tensor at that location. A common simplification is to treat the fluid as inviscid and allow slip along the tube interior surface with vanishing shear stress in the fluid. For simple boundary shapes and small amplitude motion, the coupling can be implemented analytically by linearizing the location of the boundary. For complex boundary shapes and large amplitude motions, numerical methods (see the discussion in Arienti et al., 2003) are needed to define the boundary location and couple the fluid and solid simulations.

A special case of coupled motion is small amplitude or acoustic waves in the fluid and elastic vibrations of the solid. This situation has been extensively considered in the context of underwater sound (Junger and Feit, 1986), aeroelasticity and aerodynamically generated sound (Howe, 1998). In a stationary, homogeneous, ideal (inviscid) fluid, the flow can be derived from a velocity potential ϕ that satisfies the wave equation. For axisymmetric situations, the flow is two dimensional (x, r) and there are only two velocity components (u, v).

Fluid acoustics:

[1] A complication that is observed in the present tests is cavitation (Trevena, 1987), the generation of cavities or bubbles when tension (negative pressure) occurs due to wave interactions in a liquid-filled tube. This can result in the separation of tube interior wall from the liquid as well as interior cavities. Although of great importance in water hammer (Wylie and Streeter, 1993, Watters, 1984) and underwater explosions (Kedrinsky, 2005), we have omitted discussion of that aspect of FSI from this review.

$$P' = P - P_o = -\rho_o \frac{\partial \phi}{\partial t} \,, \tag{36}$$

$$\rho' = \rho - \rho_o = P'/a_o^2 \,, \tag{37}$$

$$\mathbf{u} = (\mathrm{u}, \mathrm{v}) \,, \tag{38}$$

$$= \nabla \phi \,, \tag{39}$$

$$\nabla^2 \phi - \frac{1}{a_o^2} \frac{\partial^2 \phi}{\partial t^2} = 0 \,. \tag{40}$$

Consistent with the inviscid character of acoustic motion, the fluid-solid coupling is reduced to a *kinematic condition* that enforces the continuity of normal velocity at the fluid-solid boundary but allows the tangential velocities to differ or *slip*. The coupling occurs at the inner wall of the tube, $r = R(t)$, but this is usually linearized to be the nominal fixed radial location $r = R_o$ in acoustic analysis used in combination with the shell treatment of the tube.

Fluid-Solid Coupling:

$$\frac{\partial w}{\partial t} = \mathrm{v}(x, r = R_o, t) \,, \tag{41}$$

$$= \left. \frac{\partial \phi}{\partial r} \right|_{r=R_o} \,. \tag{42}$$

For an inviscid fluid model, only the normal component of the stress is continuous at the fluid-solid boundary so the normal stress in the solid is balanced by the pressure in the fluid. For the shell model and the acoustic solution for fluid, this condition specifies the loading which is the driving force in the shell radial motion equation.

$$\Delta P = P'(x, r = R_o, t) \,, \tag{43}$$

$$= -\rho_o \left. \frac{\partial \phi}{\partial t} \right|_{r=R_o} \,. \tag{44}$$

Skalak (1956) first solved the complete axisymmetric model for shell vibrations coupled to acoustics through these relationships. The shell model he used was a variation on (27) and the acoustic solution considered both radial and longitudinal modes. The shell model was reduced to pair of partial differential equations (fourth-order in space, second order in time) for radial and axial displacements. These two equations are coupled through the Poisson effect so that both axial and hoop strains are produced in an initial value problem that simulates projectile impact or water hammer. Skalak predicted that there are two principal sets of waves that can be

observed. A weak axial strain wave precursor moving at the bar speed runs ahead of the main pressure and hoop strain disturbances, which are moving at close to the Korteweg speed. Skalak gives an approximate analytic solution to an initial-value problem similar to projectile impact but the expressions are quite complex and almost all subsequent research on water hammer has used either the simplified version of his model (discussed subsequently) or numerical simulations of the full equations.

3.2.1 Simplified FSI models

In his 1956 paper, Skalak introduced a simpler model that is more realistic than the Korteweg model but less complex than the full coupled 2-D shell-acoustic model. This "four-equation" model has been successfully applied (Tijsseling, 1996, 2003, 2007) to a number of water hammer problems, demonstrating reasonable agreement with measured pressures and strains. The model is a straightforward extension of the Korteweg model to include axial wave propagation and Poisson coupling between radial and axial deformation. The fluid modeling assumptions are identical to the Korteweg model, neglecting bending stresses, shear effects, rotary and radial inertia. The fluid equations are identical to (8) and (9) and the acoustic approximation is used to relate pressure and density changes in the fluid. The area change is computed in terms of the change in tube radius, which is equivalent to the coupling relationship (41),

$$\frac{1}{A}\frac{\mathrm{d}A}{\mathrm{d}t} = \frac{2}{R}\frac{\partial w}{\partial t} \, . \tag{45}$$

The governing equation set reduces to two equations for the axial fluid motion, one wave equation for axial tube motion and the static force balance for the radial motion of the tube. The variables are only a function of axial distance x and time t for the simplified model, and the equations are hyperbolic, enabling solutions by standard wave propagation techniques such as the method of characteristics (Wiggert et al., 1987, Li et al., 2003) or Godunov (Gale and Tiselj, 2008) methods.

The "Four-Equation" Model:

$$\frac{1}{a_f^2}\frac{\partial P'}{\partial t} + \rho_o \frac{\partial \mathrm{u}}{\partial x} + \rho_o \frac{2}{R}\frac{\partial w}{\partial t} = 0 \, , \tag{46}$$

$$\rho_o \frac{\partial \mathrm{u}}{\partial t} = -\frac{\partial P'}{\partial x} \, , \tag{47}$$

$$\frac{\partial N_{xx}}{\partial x} = \rho h \frac{\partial^2 u}{\partial t^2} \, , \tag{48}$$

$$\frac{N_{\theta\theta}}{R} = P' \, . \tag{49}$$

Skalak explored the consequences of this model and showed that the equation set admits steady traveling waves with two eigen-speeds c_1 and c_2 that coincide with the principal speeds of the full model. The higher speed c_2 is approximately the speed of axial waves in the tube wall $\sqrt{E/\rho_s(1-\nu^2)}$ and the lower speed c_1 is approximately the Korteweg wave speed given by (21). In addition, the amplitude of the deformations and fluid velocities (relative to the fluid pressure) are the same in the reduced and full models. In particular, the peak pressure and fluid velocity in a steadily traveling wave of speed c are related by

$$P' = \rho c \mathrm{u}' \,, \tag{50}$$

which is an extension of usual acoustic relation for fluids $P' = \rho a_f \mathrm{u}'$.

One key difference is that the full model is dispersive and sharp wave fronts will spread out with time (Tijsseling et al., 2008) whereas in the reduced model, the fronts remain sharp. The main physical effect responsible for dispersion is radial inertia with bending stiffness playing a secondary role.

3.3 Thin, flexible tube $\beta \gg 1$

If the tube wall is sufficiently flexible then the compressibility of the fluid is negligible compared to the effective compressibility due to the extension of the tube. In this limit, the propagation speed is determined solely by the inertia of the fluid and the elastic properties of the tube,

$$c \approx \sqrt{\frac{A_o}{\rho_f}\frac{\partial P'}{\partial A}} \,, \tag{51}$$

which can be simplified using the relationship (15)

$$c \approx \sqrt{\frac{E}{\rho_f}\frac{h}{2R}} \,. \tag{52}$$

In the field of arterial wave mechanics (Parker, 2009), relationship (52) is generally known as the Moen-Korteweg equation. For thin tubes, this speed is quite a bit lower than the bar speed (22) or thin-tube axial wave speed since

$$c \approx a_b \sqrt{\frac{\rho_s}{\rho_f}\frac{h}{2R}} \,. \tag{53}$$

This is the limit often considered in connection with flow in blood vessels and peristaltic pumping in the intestinal tract (Grotberg and Jensen, 2004). This propagation

of extension waves in the arteries is responsible for the phenomenon of "pulse" that is used to sense the frequency of the heart beat. The pressure pulse generated by the pumping of blood into the aorta from the heart creates a propagating wave that moves with a speed on the order of 3-6 m/s near the heart and further away, as the arteries become smaller, the speed increases up to 15-35 m/s. In the case of the venous system, the effect of external pressure can lead to the phenomenon of "collapse" which will restrict the flow of blood. The collapse of a flexible, fluid-filled tube is a type of buckling instability and leads to a highly non-circular tube cross-section and a nonlinear relationship between pressure and area.

Beam (1968) carried out a novel analysis of the incompressible fluid limit using a Lagrangian formulation of the dynamics and considering large amplitude deformation of the tube wall. Treating the motion as fully nonlinear, Beam was able to determine conditions under which compression waves would steepen to form shock-like disturbances in the pressure pulses within the arteries. He formulated the hypothesis that these shock waves were the origin of the high-frequency Korotkoff sounds that are the basis of indirect blood pressure measurement (sphygmomanometer) using a pressurized cuff and a stethoscope.

4 Experimental Results

Impulsively excited wave propagation in fluid-filled tubes has been studied for shock and detonation waves inside metal tubes filled with gas or water. These studies have examined both the elastic and plastic deformation in the tubes. We have selected several examples to illustrate the cases of small $\beta \ll 1$, moderate $\beta \sim 1$, and large $\beta \gg 1$, fluid-solid coupling. .

4.1 Small coupling

This is the case of a detonation or shock wave in a gas within a thin-wall metal tube. The value of β is small (less than 10^{-3}) and there is minimal fluid-solid coupling in the sense discussed above. An ideal detonation wave propagates with a constant speed, the Chapman-Jouguet (CJ) velocity and there is a rapid pressure increase across the wave followed by a decay to a constant value. An ideal shock wave loading would be in the form of a constant velocity wave followed by a constant pressure. The pressure behind the wave front is imposed in an axially-symmetric fashion on the tube wall and excites oscillatory deflections in the tube wall. Due to the lack of coupling between fluid and solid motion, there is essentially no influence of the tube motion on detonation wave speed or flow behind the detonation. Therefore, the effect of an internal shock or detonation wave on the tube is to provide a traveling or moving load applied at the interior tube surface in the radially outward direction.

The problem of a traveling internal load on a tube has been extensively examined (see Beltman et al., 1999, Beltman and Shepherd, 2002) and in the simplest formulation is equivalent to a traveling load imposed on a beam supported by an elastic foundation. Considering the tube as a thin-shell, there are four axisymmetric modes of tube motion (Tang, 1965) that are generated in this case. In order of increasing wave speed, these are the flexural waves, shear waves, bar waves, and longitudinal waves. The flexural wave exhibits the largest amplitude of tube hoop strain and is the most significant of all of these modes. Flexural waves, like other structural modes, do not have a well-defined wave speed but are dispersive and the main wave front moves at a phase velocity that is equal to the speed of the loading front (shock or detonation wave speed). For weak shock waves, this is the acoustic speed in the gas so that the flexural wave corresponds to the $\beta \to 0$ limit of the Korteweg wave mode of acoustic disturbances. For strong shock waves or detonations, the wave speed in gas may significantly exceed the gas acoustic speed and this may excite very strong deflections in the tube for certain speed ranges. In particular, there is a pronounced resonance (Beltman et al., 1999, Beltman and Shepherd, 2002, Chao and Shepherd, 2005b) when the phase speed is equal to the group velocity and large amplitude hoop strain oscillations can be observed in this situation.

For a given pressure behind the gas wave, the maximum hoop strain is a function of the wave speed relative to the critical speed or group velocity of the flexural waves. Chao and Shepherd (2005b) examined the possibility of additional resonance at the modified shear wave speed in the shell but did not observe any amplifications of hoop strains in this speed range in agreement with the Tang model and finite element simulations. Amplification of the shear strains is predicted (Chao and Shepherd, 2005b) but the effect is modest in comparison with the flexural wave resonance. Additional resonances at even higher speeds, in the range between the bulk sound speed and dilatation speed, are observed in finite element numerical simulations by Lewis and Nechitailo (2007). It will be difficult to experimentally observe these effects in gases with metal tubes but it may be possible in plastic tubes with the additional complication of viscoelastic behavior.

4.2 Elastic motions

Fig. 2a shows gaseous detonation pressure histories measured at intervals of 127 mm along the axis of a steel tube 1.25 m long and 127 mm inside diameter with a 12.7 mm thick wall, (see Liang et al., 2006a, for details). Fig.2b shows the hoop strain histories at the corresponding axial locations. Comparing the two plots, we can see that the main flexural wave front moves at the speed of the detonation front, about 2090 m/s. A small amplitude precursor can be observed moving ahead of the main wave front, the leading edge of the precursor travels at about 5000 m/s, close to the bar wave speed in the tube. The hoop strain oscillations have a frequency of f_h = 17.5 kHz, which corresponds to the hoop or breathing mode associated with a purely radial motion. The amplitude modulation of the hoop oscillations is mainly

to the superposition of oscillations created by the incident detonation and reflected shock wave with additional disturbances created by the welded-on pressure gage ports. The tube is stiff and the peak pressures are relatively modest so that the peak strains are less than 250 μstrain ($\varepsilon \leq .00025$) and all motion is purely in the elastic regime. A more ideal response can be obtained by carrying out tests with a section

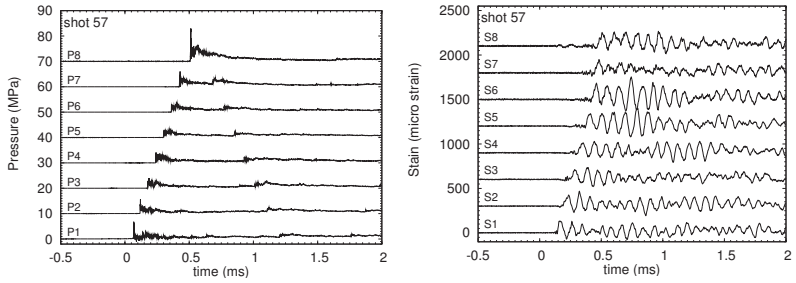

(a) (b)

Fig. 2 Elastic structural response of a steel tube to a gaseous detonation. a) pressure histories. b) strain histories (bonded strain gages) (Liang et al., 2006a).

of tube with a uniform cross-section and carefully-controlled boundary conditions (Shepherd et al., 2008, Liang et al., 2006b). Nearly sinusoidal oscillations in radial deflection with constant amplitude can be observed in Fig. 3. The specimen tube is 6061T6 aluminum, the same type used as in previous studies. Outer diameter is 41.28 mm (1.625 in). The thickness of the tube is nominally 0.89 mm (0.035 in) but actual dimensions vary by +/- 10% due to the manufacturing technique. The tube was held by collets spaced 420 mm apart and the measuring location was halfway between the collets.

4.3 Plastic motions

If the tube wall is sufficiently thin and the shock or detonation pressure sufficiently high, plastic deformation of the tube will occur (Smith, 1986, 1990). When this happens, the radial deflection of the tube is dominated by the resulting permanent deformation and the oscillations that are so prominent in the elastic case are negligible compared to the plastic deformation. Fig. 4 shows a set of hoop strain histories measurements for the same internal dimensions as shown previous, 1.24 m long tube and 127 mm inner diameter, but with a wall thickness of 1.5 mm. The detonation wave occurred in a stoichiometric methane-oxygen mixture at an initial pressure of 0.35 MPa (Pintgen and Shepherd, 2006).

Because of these differences, the peak strains in this case are almost 100 times larger than in the elastic case shown previously. The steel is a mild carbon steel

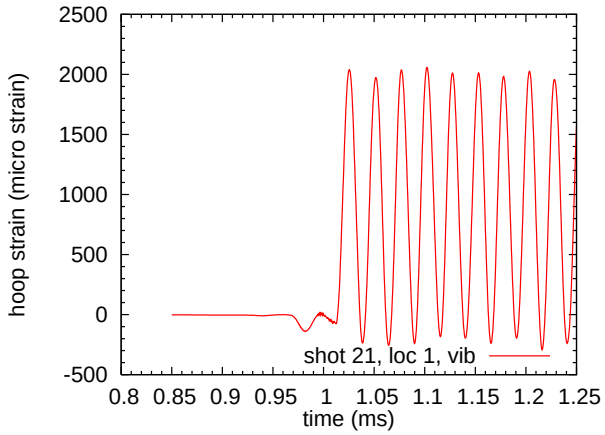

Fig. 3 Elastic structural response of a thin-wall aluminum tube to a gaseous detonation as measured by a optical displacement interferometer (Shepherd et al., 2008).

(C1010) which exhibits significant work hardening and strain rate effects that must be considered in order to predict the extent of the deformation. Very rapid changes in deformation are created by both the incident detonation and reflected shock wave. The reflected shock decays rapidly as it moves away from the reflecting end so that two distinct waves are particularly visible for the gage at 1.13 m. The rate of change of the tube radius is limited primarily by inertia and on the time scale shown, the rise time is relatively short so that the waves appear nearly as a step change ("plastic shock wave"). If there is sufficient deformation to reach the tensile limit, rupture and fragmentation can occur. Rupture due to gaseous detonation can occur under extreme loading conditions that are created by transition from deflagrations (flames) to the detonation mode of combustion (Shepherd, 2009). The related process of crack propagation from pre-existing flaws has been studied for detonation loading in a series of experiments by Chao (2004).

4.4 High Explosives

There has also been a substantial amount of research, for example, by Duffey and Mitchell (1973), Benham and Duffey (1974), Hodge (1956), Duffey (1971), Duffey and Krieg (1969), Fanous and Greiman (1988) and others cited in the review by Florek and Benaroya (2005), on the plastic response of tubes to high explosives. This is of great practical interest for confining explosions (Rodriguez and Duffey, 2004, Duffey et al., 2002) for purposes of testing or transporting explosive materials. However, these situations typically involve concentrated energy releases and do not result in propagating deformation waves. A single bulge in the tube is typically

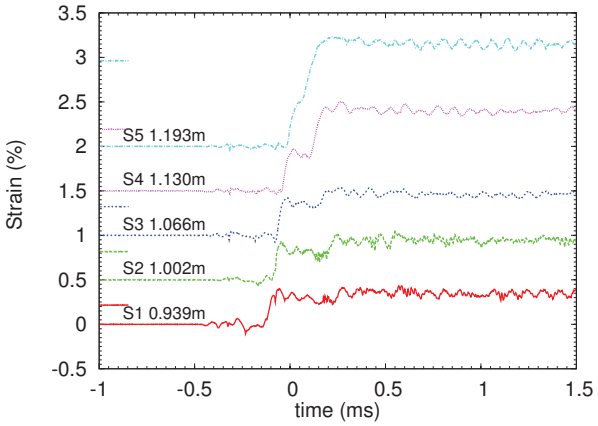

Fig. 4 Plastic structural response (hoop strain) of a thin-wall steel tube to a gaseous detonation as measured by bonded strain gages. The short data lines at the left side of the figure indicate the final residual plastic deformation (Pintgen and Shepherd, 2006).

created by the explosion unless the energy release is sufficient to fracture the tube. For high explosives in air-filled tubes, it is possible to predict the final deformation using approximate equations of motion when strain rate and strain hardening effects are taken into account. Similar experiments in water-filled tubes (Sandusky et al., 1999, Chambers et al., 2001) have been carried out to provide data on wall motion and internal pressure that can be used to validate simulations of underwater explosions (Wardlaw and Luton, 2000). Plastic deformations as large as 20% were recorded in the middle portion of a 100 mm diameter aluminum (type 5086) tube with a 5.35 mm wall thickness.

5 Moderate coupling

Experiments have been carried out at CIT (Inaba and Shepherd, 2008a,b) to create impact-generated stress waves in a water-filled tube using the configuration shown in Fig. 1. A 700 g steel projectile was accelerated by compressed air through a 1.5 m long barrel and impacted a polycarbonate buffer at the top of the tube. The projectile velocity and impact dynamics were recorded with high-speed photography. The buffer accelerates impulsively as soon as it is impacted by the steel projectile, decelerates to a stop in about 1 ms and reverses direction. The buffer is sealed to the tube with two o-rings to prevent the water from squirting through the small gap between the buffer and tube.

A sharp pressure pulse (Fig. 5) is created by the initial impulse due to the impact of the projectile followed by an approximately exponential decay in time of pressure due to the expansion waves generated as the projectile slows down. An elementary

theory of the pressure pulse generation mechanism is given in the Appendix. The incident pressure wave propagates down the tube with the Korteweg wave speed, reflects from the bottom closure of the tube with an increase in amplitude, then propagates back up to the buffer. When the compression wave reflects from the free surface of the buffer, a tension wave is generated that propagates into the water resulting in cavitation.

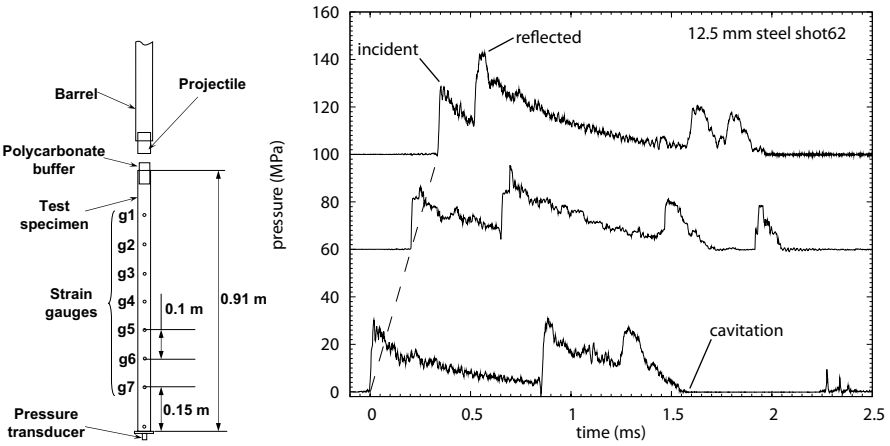

Fig. 5 Pressure waves generated by projectile impact on a water-filled steel tube with a 12.5 mm thick wall (Inaba and Shepherd, 2008a).

5.1 Elastic Waves

For sufficiently low projectile velocities and/or sufficiently thick tubes, the structural deflections are elastic. Operating in this regime and using commercial metal tubes, we can test the conventional models based on water-hammer theory. The pressure waves in the fluid are accompanied by longitudinal (axial) and hoop strain waves in the tube wall. To observe these waves, Inaba and Shepherd (2008a) used thin-wall mild steel tubes (1020 type, 0.91 m long, 40 mm in diameter, 0.77 mm wall thickness) instrumented with bonded strain gages at 10 cm intervals (Fig. 6). In agreement with the theory of Skalak (1956), the bulk of strain (primary wave) is in the hoop direction and traveling at the Korteweg speed in phase with the pressure pulse. A small-amplitude longitudinal tension wave (precursor wave) propagates at the thin-plate velocity

$$c_p = \sqrt{\frac{E}{\rho_s(1-\nu^2)}}\,, \tag{54}$$

ahead of the main disturbance. A much larger amplitude longitudinal compression wave propagates in phase with the main hoop signal due to the Poisson effect. In agreement with the linear theory, shown in Fig. 7, the precursor wave speeds are independent of the impact velocity and peak strain amplitudes scale linearly with impact speed. The effect of tube wall thickness on primary wave speed is in agreement with either the thin- or thick-wall models but in order to accurately predict hoop strain on the outside of the tube, the radial distribution of stress has to be taken into account (Watters, 1984, Tijsseling, 2007).

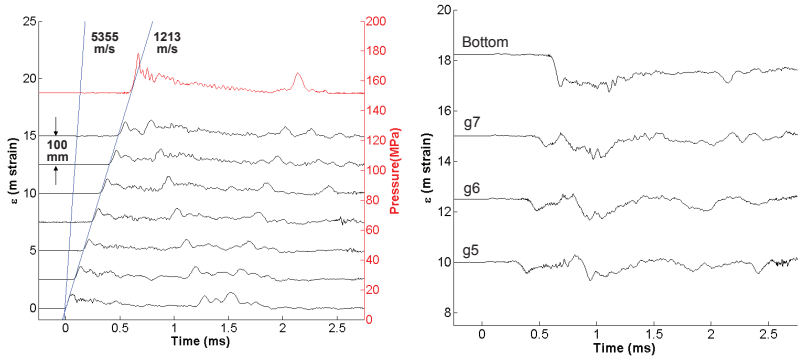

(a) (b)

Fig. 6 Elastic deformation waves generated by projectile impact on thin-wall water-filled steel tube (Inaba and Shepherd, 2008a); a) hoop strain, b) longitudinal strain.

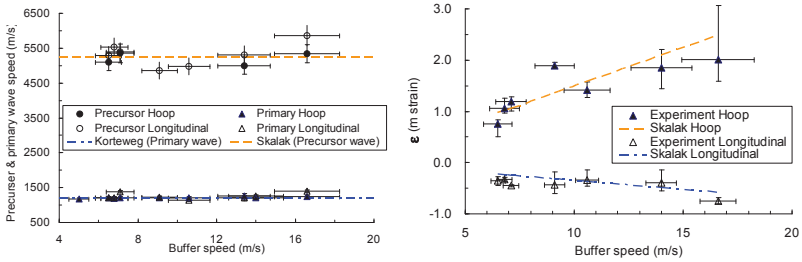

(a) (b)

Fig. 7 Elastic wave properties for projectile impact on thin-wall water-filled steel tubes (Inaba and Shepherd, 2008a). a) Wave speeds and b) primary hoop and longitudinal strain peak amplitudes compared with Skalak (1956) model.

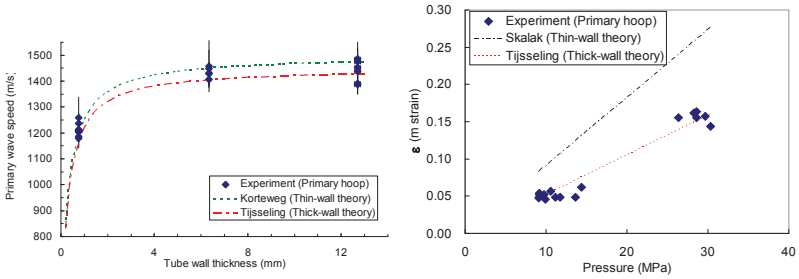

Fig. 8 Elastic wave properties for projectile impact on water-filled steel tubes (Inaba and Shepherd, 2008a). Effect of wall thickness on a) primary wave speed and b) peak hoop strain. Comparison with Skalak (1956) and Tijsseling (2007) models.

5.2 Plastic deformation

By using higher impact velocities, plastic deformation of the tube and in extreme cases, rupture, can be observed. For example, (Inaba and Shepherd, 2008b) have observed, Fig. 9, plastic deformations with peak hoop strains up to 0.4% in a thin-wall aluminum (AL6061-T6) tube with a projectile velocity of 16 m/s. The tube was seamless, had a nominal wall thickness of 0.86 mm, inner diameter of 39 mm, and was $\sim$0.9 m long. The incident wave front speed derived from Fig. 9 (a) is 946 m/s which is close to the value of 960 m/s predicted by the classical Korteweg theory (Table 2).

In the test shown in Fig. 9, the tube ruptured just above the closure at the bottom of the tube. This is not surprising since the highest pressures and strains occur at this location due to the interaction of the incident and reflected waves. The onset of tube rupture is indicated by a sudden pressure decrease at 0.5 ms which propagates up the tube as a pressure expansion wave and associated strain signals, Fig. 9a. Under the conditions of the testing for this specimen, rupture did not occur until after the 9th test and sufficient damage has accumulated to create a through wall crack. The crack only propagated a limited distance (50 mm), Fig. 9b, before arresting due to the loss of driving force associated with the flow of fluid out of the crack and rapid depressurization of the tube.

The rupture behavior is very similar to what was previously observed (Chao and Shepherd, 2004) in the rupture under static loading with hydraulic fluid of an identical tube specimen with a deliberate flaw used to initiate fracture. As discussed by Chao and Shepherd (2004), the limited extent of the rupture under hydraulic as compared to pneumatic (pressurized gas) loading is a consequence of two factors. First, for a given pressure, a much smaller amount of energy per unit volume can be stored in a compressed liquid than a gas. Second, with liquid pressurization the crack driving force decreases below the critical level required to create new fracture surfaces much more rapidly than for gaseous pressurization.

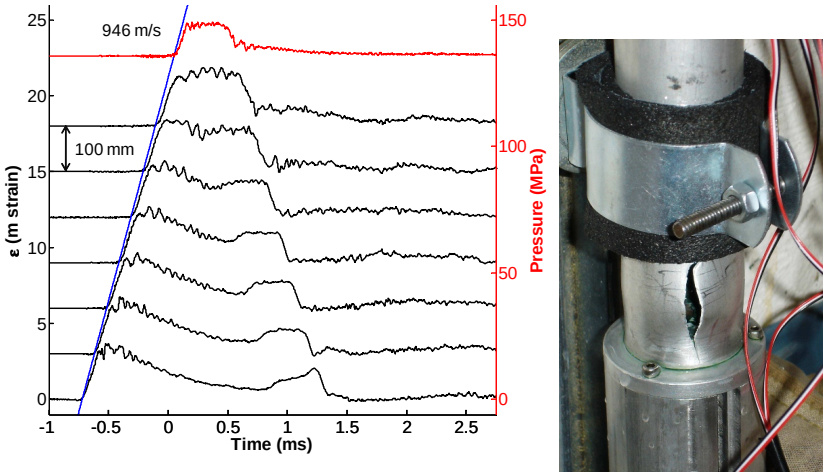

(a) (b)

Fig. 9 Deformation in plastic regime and rupture generated by projectile impact on a water-filled aluminum tube (Inaba and Shepherd, 2008b). a) hoop strain and pressure histories and b) tube rupture at the tube bottom. Impact speed 15.8 m/s, 50 mm rupture length.

Strains can be observed that are greatly in excess of the nominal elastic proportional limit (ε = .002) in tests with more ductile tubes and higher projectile velocities. Using a new vertical gas gun facility we constructed in our laboratory at the California Institute of Technology, we have carried out experiments with projectile speeds up to 100 m/s. Hoop strain and pressure histories are shown in Fig. 10 for a 65 m/s impact on a water-filled 1.59 mm thickness, 40.0 mm inner diameter, 0.9 m long mild steel tube. The precursor and primary wave velocities are 5219 and 1346 m/s, respectively. Despite the very large (up to 16%) permanent deformations that occur in this test, the observed wave speeds are in reasonable agreement with the Skalak (1956) model predictions of 5226 m/s and 1337 m/s. This good agreement is apparently a consequence of the limited deformation that takes place in the precursor and primary waves, making the elastic assumption of the Skalak model a reasonable approximation.

A relatively long time is required to reach the ultimate plastic deformation as compared to the initial elastic deformation waves. The situation appears to be very similar to that of uniaxial stress waves in shock compression (see Ch. 3 of Meyers, 1994): An elastic precursor wave with an amplitude given by the proportional limit travels at the elastic longitudinal wave speed in front of a lower speed plastic wave with a continuous increase in strain (stress) up to the final level of permanent deformation. In the case of the water-filled tube, Fig. 10b, significant attenuation of the plastic wave is observed with increasing distance from the impact point. This occurs in uniaxial shock compression testing due the attenuation of a following expansion

wave. In the present case, we speculate that there are multiple factors including not only the expansion wave but also the radial motion of the tube wall and the energy absorption due to plastic work. Although the Korteweg theory can be naively extended to plastic deformation, the dispersive nature of the plastic deformation waves suggests that radial motion, fluid and tube inertia effects may also be significant in the plastic case and the simplifying assumptions of the Korteweg theory may not be valid in the case of large plastic deformation.

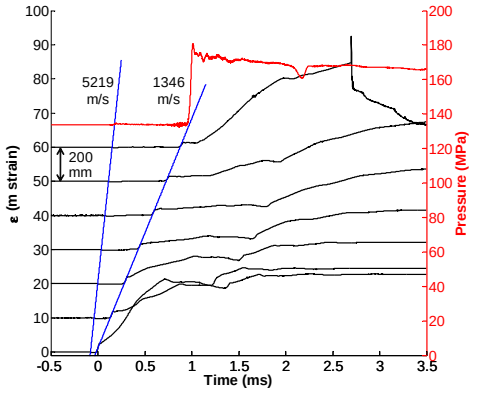

(a)

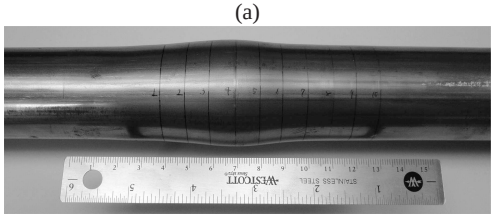

(b)

Fig. 10 Large plastic deformation generated by projectile impact on a water-filled steel tube. a) hoop strain and pressure histories and b) bulge (16% maximum strain) near the location of the bottom of the buffer. The initial buffer speed following impact was 62.7 m/s.

5.3 Composite and Polymer tubes

The strain waves observed in metal tubes are relatively straightforward to interpret, with distinct incident and reflected waves. The waves in composite and polymer tubes are more complex. This is due to the anisotropic nature of the the roll-wrapped and filament wound composite tubes that we have used in our tests as well as the viscoelastic nature of the polymer tubes and matrix materials. Although many fea-

tures in the strain waves are different, the results from composite and polymer tubes do share a common feature with the metals of a distinct strain front that propagates with a speed much lower than either fluid or structural wave speeds. If we define an effective modulus (Hull and Clyne, 1996, Spencer and Hull, 1978) for the hoop response, the general ideas of the Korteweg theory still appear to be relevant and useful for interpreting the results of experiments. As an example, consider the test on a roll-wrapped carbon-fiber composite (CFC) tube shown in Fig. 11. This tube consisted of a longitudinal fiber core with a woven cloth over-wrap and vinylester resin and has a 1.45 mm thickness wall, 38.2 mm inner diameter, and is 0.9 m long. The speed of the strain wave front in Fig. 11a is 864 m/s, substantially lower than observed in metals and consistent with the lower hoop stiffness for tubes with this construction method.

For metal tubes, the longitudinal and hoop strains are strongly correlated and positive strains in the hoop direction result in negative longitudinal strain. The sign and the magnitude (longitudinal strain is about -1/3 of the hoop strain) is the expected result based on the Poisson effect for an isotropic material. For the roll-wrapped CFC tube, the longitudinal strain shown in Fig. 11b is a much smaller fraction of the hoop strain ($\sim$0.1) than for the aluminum tubes. This is due to the decoupling of the longitudinal and hoop stress carrying ability since the majority of the carbon fibers and load carrying capability are in the longitudinal direction for this tube.[2]

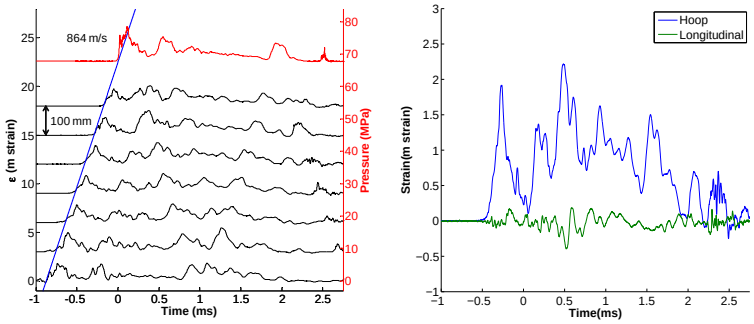

(a) (b)

Fig. 11 Strain waves generated by projectile impact on a water-filled roll-wrapped CFC tube. a) hoop strain and pressure histories and b) hoop and longitudinal histories located at the same distance from the tube top. The impact speed was 7.7 m/s.

As expected for this method of construction, the roll-wrapped tubes are relatively weak in the hoop direction and failed under modest impact velocities, see Fig. 12. Rupture occurred near the tube bottom and creates a distinct release wave in the

[2] Recent testing with filament-wound CFC tubes show that the allocation of strain between hoop and longitudinal directions is a systematic function of the winding angle as expected from the theory of Puck (see Greenwood, 1977) and quite different than in the roll-wrapped case.

strain histories (Fig. 12). The rupture event is much more dramatic than in aluminum since the failure in CFC is by a high-speed brittle fracture rather than the quickly-arresting ductile rupture that is observed in the aluminum tubes. Rupture of the CFC tube occurred on the first high impact speed test while the ductility of the aluminum tube delayed rupture until the damage had accumulated from a number of successive impacts.

The roll-wrapped CFC tube rupture was in the form of a long, straight crack parallel to the tube axis and serendipitously intersected the longitudinal strain gages so that the strain signals can be used to deduce the apparent crack tip speed to be about 2000 m/s, These are much higher than typical crack tip speeds of 200-300 m/s observed (Chao and Shepherd, 2004, 2005a) in detonation-driven fracture of aluminum. However, this value is actually quite a bit lower than crack tip velocities of up to 7000 m/s that were observed by Coker and Rosakis (2001) in impact experiments on mode I and II cracks in unidirectional graphite-epoxy composite plates. As discussed in Chao and Shepherd (2004), the cracks in internally-pressurized tubes initiate in Mode I since the major principal stress is in the hoop direction, perpendicular to the initial crack tip motion. However, in thin ductile tubes, the plastic deformation of the material adjacent to the crack quickly results in a transition to mixed mode fracture (Chao and Shepherd, 2005a).

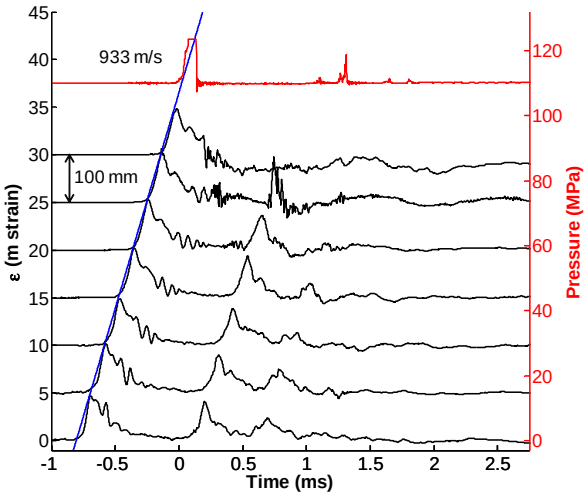

Fig. 12 Hoop strain and pressure histories generated by projectile impact on a water-filled roll-wrapped CFC tube. This tube failed by fracture near the bottom just after reflection of the pressure wave.

The roll-wrapped CFC tubes always burst near the bottom boundary[3] in the tests with higher driver pressures while a filament-wound glass-reinforced plastic (GRP) tube survived intact under these same conditions. The GRP tube has a 1.60 mm thickness, 38.8 mm inner diameter, 0.9 m long with a winding angle of 40 degrees. The hoop strain histories shown in Fig. 13 for the GRP tubes are similar to those of the CFC tubes. Longitudinal strain histories shown in Fig. 13b for the GRP tube are correlated to hoop strains similar to those in the Al tubes, in contrast to the CFC tubes. The primary wave velocity measured for the hoop strain wave front is 904 m/s, similar to the speeds in the roll-wrapped CFC tubes. In Fig. 13b, peak hoop strains greater than 0.7% were observed but residual strain near the reflecting boundary is still negligible after the experiment. The primary flexural wave velocities are 949 m/s, slightly faster than those in Fig. 13a.

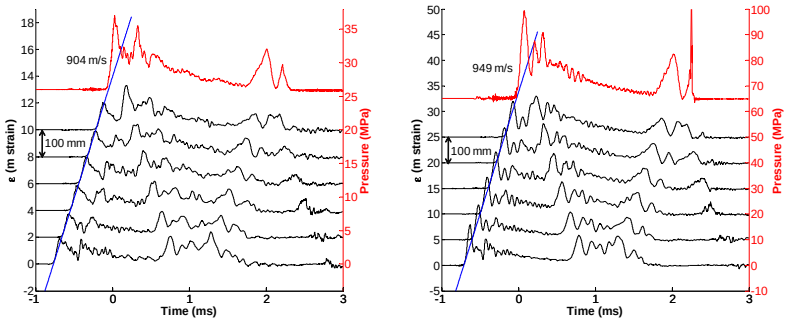

(a) (b)

Fig. 13 Hoop and pressure histories generated by projectile impact on a water-filled GRP tube. a) impact speed 6.8 m/s and b) impact speed 18.8 m/s.

The polycarbonate tube (PC) is more flexible and exhibits more significant fluid-solid coupling than either metal or composite tubes. The PC tube we tested is a transparent tube with a 6.4 mm thick-wall and a 38 mm inner diameter. Limited results are available since the primary purpose of these tests were to visualize cavitation. The primary wave propagates at 552 m/s, Fig. 14, much slower than waves in metal or composite tubes. The bar sound speed of the PC tube is estimated to be 1386 m/s using a density of 1250 kg/m^3 and Young's modulus 2.4 GPa. The coupling parameter β deduced from the Kortweg model and observed primary wave speed is 6.3, which implies an effective Young's modulus of 2.4 GPa, in agreement with the material properties despite the known viscoelastic nature of wave propagation in PC.

[3] Recent testing with filament-wound CFC tubes show that rupture can occur either at the bottom of the tube or at sufficiently high velocities, just below the buffer. As expected, the filament-wound tubes are much stronger under hoop loading than the roll-wrapped construction and the failure mode is quite different.

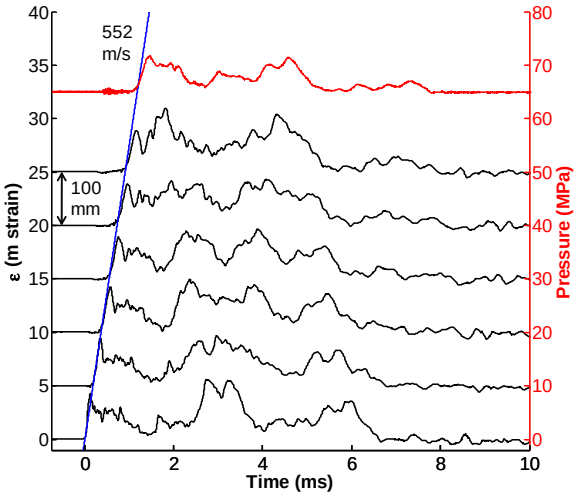

Fig. 14 Hoop and pressure histories generated by projectile impact (6.4 m/s) on a water-filled PC tube.

Measured primary stress wave velocities for four materials are summarized in Fig. 15. There is no clear correlation of wave speed with impact velocity and given the modest wave amplitudes, we expect to be in the linear regime with constant wave speeds. There are no published theoretical treatments for general composite materials although (Pinnington, 1997) treats the related problems of a wire reinforced hose. Based on the experimentally measured wave front speed of about 900 m/s for elastic flexural waves in CFC and GRP tubes, the effective coupling parameter can be computed using the simple Korteweg model to be about 1.81 and 1.75, respectively. The tensile modulus of the carbon epoxy composite (CFC) is typically 140 GPa along the fiber direction while effective modulus derived from the present tests is 33 GPa. This is consistent with a relatively low Young's modulus in the hoop direction of the roll-wrapped CFC material which is to be expected since the majority of the carbon fibers are aligned in the longitudinal direction. According to (Watters, 1984), the elastic modulus for common GRP pipe is 27.6 GPa and is close to the effective Young's modulus derived from the present tests with the GRP tube (32 GPa).

6 Summary

Stress wave propagation in water-filled tubes provides a framework for studying different aspects of fluid-solid coupling than the standard normal shock impact on

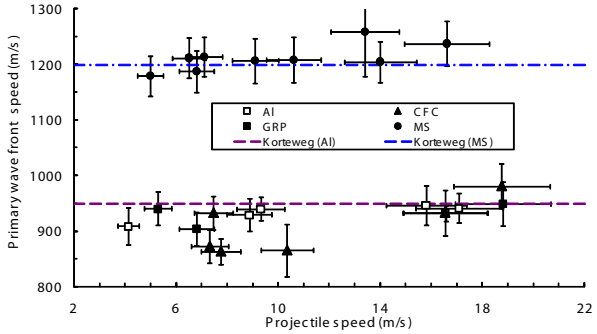

Fig. 15 Primary stress wave front speed as function of projectile speed. Al and mild steel (MS) wave velocities are compared with the Korteweg theory.

underwater structures. There is already a substantial amount of analysis available for the elastic motions that can be borrowed from the engineering problem of water hammer. The key result of both analysis and experiments is that large amplitude coupled solid stress waves and fluid pressure waves can be excited in a relatively simple configuration. The solid motion is in the form of traveling waves that move axially along the tube when the excitation is projectile impact on the water surface at one end of the tube. The primary flexural waves propagate much slower than either the sound speed in water (1500 m/s) or tube bar speeds (Al 5100 m/s, MS 5200 m/s, CFC 9500 m/s, GRP 5300 m/s). This is due to the flexural motion in tube being strongly coupled to compression wave in water. In the context of elastic motion, this coupling is controlled by a single parameter that is a function of the tube stiffness, fluid compressibility, and densities of the fluid and tube materials.

For tubes constructed of isotropic elastic materials, theories are available to predict the observed wave speeds and amplitudes. Using the simplest version of the theory, due to Korteweg, the predicted primary wave speeds are 950 m/s for Al and 1200 m/s for mild steel, which are in good with our experimental results. More sophisticated models predict the presence of an axial strain wave precursor, which we have also observed. Similar primary waves are also observed in tubes constructed from composite materials and the wave speeds are consistent with estimated stiffness although there is limited theory for the composite cases. Plastic deformation and rupture have been observed in tests with modest projectile velocities ($<$ 100 m/s), indicating the suitability of this configuration for examining the ultimate strength and failure characteristics with this configuration of fluid-solid coupling.

Acknowledgements Studies on detonation and shock loading of gas-filled tubes were sponsored at CIT by the Office of Naval Research and the US DOE through the Academic Strategic Alliance Program, Center for Simulation of Dynamic Response in Materials. Experimental studies and analysis were carried out under these programs by Zhe Liang, Tim Curran, James Karnesky, Florian Pintgen, Tony Chao, and Marco Beltman. Studies on fluid-filled tubes are being carried out under the DOD MURI on Mechanics and Mechanisms of Impulse Loading, Damage and Failure of Ma-

rine Structures and Materials Sponsored by the Office of Naval Research, Dr. Y. D. S. Rajapakse, Program Manager. Chris Krok, Tim Curran, Kevin Zhang, and Tomohiro Nishiyama contributed to the execution and analysis of the water-filled tube experiments.

Appendix

The modeling of impact-generated pressure pulses and the approximate equation of state used for water is described.

Pressure Pulse from Projectile Impact

In order to properly determine the pressure pulse in the fluid in the most general situation, FSI must be properly included which requires simultaneously solving for motion in the confining tube and the fluid. However, in the case of a stiff tube, $\beta \rightarrow 0$, we can neglect the FSI and just consider the one-dimensional wave mechanics in the fluid and projectile.[4] This means we can make use of ideas from the classical treatments of shock wave generation and decay in solids, see Fowles (1960) and Meyers (1994). The situation we consider is shown in Fig. 18. In our experiments, a buffer is placed between the projectile and the fluid. The buffer-projectile and buffer-fluid interfaces will create additional waves that may need to be accounted for in order to make realistic predictions of the resulting pressure profile in the fluid. However, the general features of the pressure pulse can be appreciated by analyzing the simple situation of Fig. 16.

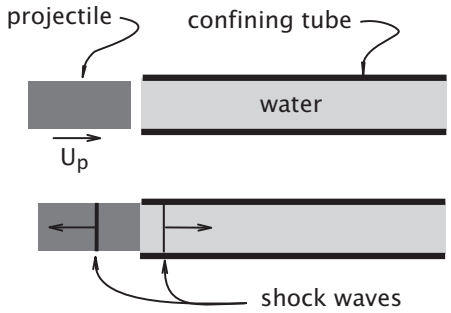

Fig. 16 Generation of initial waves in projectile and fluid by impact.

[4] Using the pressure-velocity relationship of (50) the analysis of the present section can readily be extended to include FSI.

The initial impact creates a shock wave with an amplitude determined by the impact velocity and the acoustic impedances ρa of the projectile and fluid. The pressure-velocity matching method (Meyers, 1994) can be used to construct the solution by assuming simple waves in both fluid,

$$\Delta P = (\rho a)_f \Delta \mathrm{u} \,, \tag{55}$$

and projectile,

$$\Delta P = -(\rho a)_p \Delta \mathrm{u} \,. \tag{56}$$

For the case of a steel projectile impacting water, the results are shown in Fig. 17. The pressure amplitude ΔP of the initial wave in the water is proportional to the velocity of the projectile before impact,

$$\Delta P = \frac{(\rho a)_p (\rho a)_w}{(\rho a)_p + (\rho a)_w} \mathrm{V_p} \,. \tag{57}$$

As shown, the impedance of steel is much higher than that of water which leads to the approximation,

$$\Delta P \approx (\rho a)_w \mathrm{V_p} \,. \tag{58}$$

The projectile begins slowing down immediately after impact creating expansion

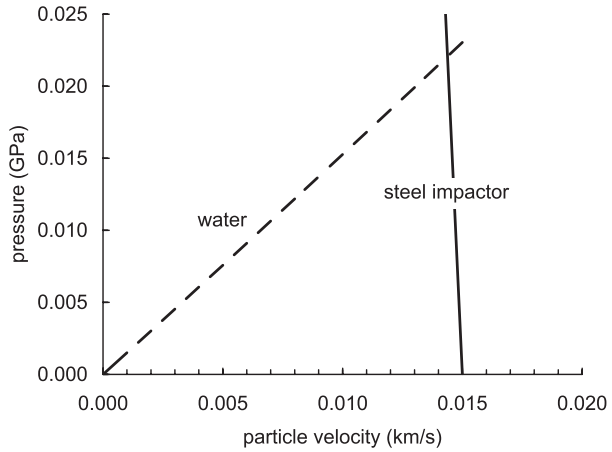

Fig. 17 Pressure-velocity diagram for computing peak pressure due to a steel projectile impacting on water. The case of a 15 m/s projectile is shown.

waves that follow the initial compression wave in the water. The water is treated as

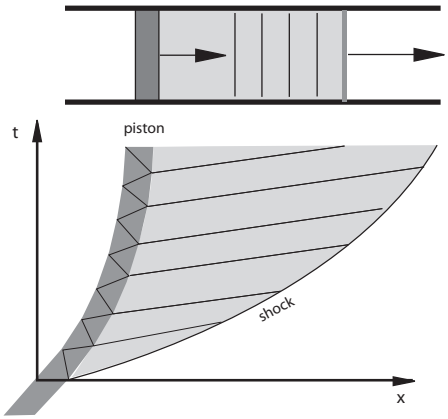

Fig. 18 Wave system created by reverberation following impact of the projectile on the fluid surface.

compressible using the Tait equation of state described in the subsequent section,

$$P = P(\rho, s) \ . \tag{59}$$

For small projectile velocities relative to the sound speed in the projectile, there are many reverberations of the waves within the projectile during the characteristic time of slowing. This means that the projectile can be approximately treated as a rigid body and treated with the methods of Newtonian mechanics. This idea has been used by a number of researchers to develop simple analytical (Deshpande et al., 2006, Espinosa et al., 2006) and numerical solutions (Skews et al., 2004) for the wave generation process. The equation of motion of the projectile is

$$M_p \frac{\mathrm{dV_p}}{\mathrm{d}t} = -A_p \left(P - P_1\right) \ , \tag{60}$$

where P is the pressure on the water face of the projectile and P_1 is the ambient pressure on the free (rear) surface of the projectile. For weak shock waves, we can treat the motion in the water as approximately isentropic so that the method of characteristics can be used to compute the relationship between sound speed a_p and fluid velocity $\mathrm{u_p}$ at the water face of the piston. For the Tait equation, this is

$$a_p - \frac{n-1}{2}\mathrm{u_p} = a_1 \ , \tag{61}$$

where n is an empirical constant with a value of 7 for water. At the face of the piston, the fluid velocity is the same as the piston velocity so that changes in the piston velocity are related to changes in the sound speed by

$$\mathrm{dV_p} = \mathrm{du_p} \,, \tag{62}$$

$$= \frac{2}{n-1} \mathrm{d}a_p \,. \tag{63}$$

For weak shock waves, the motion is isentropic and the changes in sound speed can be uniquely related to changes in pressure through the equation of state,

$$\mathrm{d}a_p = \left(\frac{\partial a}{\partial P}\right)_s \mathrm{d}P \,. \tag{64}$$

This results in a simple ordinary differential equation for the pressure difference $\Delta P_p = P_p - P_1$ at the water face of the piston,

$$\frac{\mathrm{d}\Delta P_p}{\mathrm{d}t} = -\frac{n-1}{2}\left(\frac{\partial P}{\partial a}\right)_s \frac{A_p}{M_p}\Delta P_p \,. \tag{65}$$

The solution to this is

$$\Delta P_p(t) = \Delta P_p(0)\exp(-t/\tau) \,, \tag{66}$$

where the time constant is

$$\tau = \frac{M_p}{A_p\left(\dfrac{\partial P}{\partial a}\right)_s \dfrac{n-1}{2}} \,. \tag{67}$$

The initial velocity $\mathrm{V_p}(0)$ and pressure $\Delta P_p(0)$ are determined by the initial impact analysis of (58). If we neglect the dependence of the characteristic speeds on amplitude, the temporal variation of pressure on the face of the piston will also be the temporal variation behind the wave. In experiments, the pressure behind the leading front will show a series of steps due to the discrete wave interactions at the interfaces between buffer, water, and projectile.

An example of the comparison of this model with the measured pressure is shown in Fig. 19. The peak pressure of 27.4 MPa was computed using (58) and the projectile initial speed of 18.5 m/s. A time constant of τ = 0.41 ms was computed using (67) and the projectile length of 75 mm. The model does remarkably well aside from the obvious differences in the first 200 μs due to wave motion in the buffer and projectile.

Tait Equation of State

The Tait equation of state is a simple analytic model that is useful for modeling a compressible liquid like water under modest compression. Experimental observa-

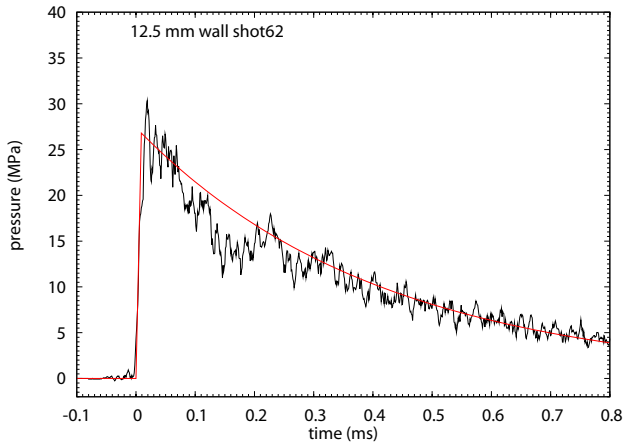

Fig. 19 Comparison of measured and model pressure for water in a 12.5 mm thick steel tube and an 0.67 kg steel impactor with an initial speed of 18.5 m/s.

tions suggest that the isentropic compressibility can be described by the following empirical formula,

$$-\frac{1}{\upsilon}\left(\frac{\partial \upsilon}{\partial P}\right)_s = \frac{1}{n(P+B)}\,, \tag{68}$$

where n and B are empirical constants, $B = 2.995 \times 10^8$ Pa and $n = 7$ for water. From the definition of sound speed,

$$a^2 = -\upsilon^2\left(\frac{\partial P}{\partial \upsilon}\right)_s\,, \tag{69}$$

we have that

$$a^2 = n\upsilon(P+B)\,. \tag{70}$$

This leads to the following differential equation for pressure,

$$\frac{\mathrm{d}P}{P+B} = -n\frac{\mathrm{d}\upsilon}{\upsilon}\,, \tag{71}$$

which can be integrated to yield

$$P = B\left[\left(\frac{\upsilon_1}{\upsilon}\right)^n - 1\right]\,, \tag{72}$$

or as a function of sound speed

$$P = B\left[\left(\frac{\rho_1 a^2}{nB}\right)^{\frac{n}{n-1}} - 1\right] . \tag{73}$$

The reference density is $\rho_1 = 953.26$ kg/m^3 and the resulting reference sound speed is $a_1 = 1483$ m/s. Using the expression for pressure, we can rewrite the sound speed as

$$a^2 = nB\upsilon_1\left(\frac{\upsilon_1}{\upsilon}\right)^{n-1} . \tag{74}$$

In the derivation of the piston motion, we need the derivative of the pressure with respect to the sound speed,

$$\left(\frac{\partial P}{\partial a}\right)_s = \frac{2n}{n-1}\frac{P+B}{a} . \tag{75}$$

Evaluating this at the nominal initial conditions, we obtain the value

$$\left(\frac{\partial P}{\partial a}\right)_s = 4.714\times 10^5\ \mathrm{Pa\cdot s\cdot m^{-1}} . \tag{76}$$

A short table of compressed water states estimated by the Tait equation are given in Table 3 for the parameters $\rho_1 = 953.263$, $B = 2.995\times 10^8$, $n = 7$.

Table 3 Compressed liquid water states estimated by the Tait equation.

a (m/s)	P (bar)	ρ/ρ_1	u_p (m/s)	U_s (m/s)
1483.3	1	1.0001	0.10	1483.20
1503	95	1.0045	6.67	1496.33
1528	216	1.0100	15.00	1513.00
1553	340	1.0155	23.34	1529.67
1578	467	1.0209	31.68	1546.34
1603	596	1.0263	40.02	1563.01
1628	728	1.0316	48.36	1579.68
1653	863	1.0368	56.72	1596.36
1678	1001	1.0420	65.07	1613.04

Shock Hugoniot for Water

Shock wave researchers conventionally represent the *Hugoniot* or locus of shock states using relationships between the fluid velocity u_p and the shock velocity U_s (Marsh, 1980). A typical empirical relationship used to correlate data is $U_s = a_o + s\, u_p$. For water, fitting the Nagayama et al. (2002) data gives the parameters of a_o = 1450 and s = 1.99. Using the shock jump conditions in the form:

$$U_s = v_1 \sqrt{\frac{P - P_1}{v_1 - v}}\,, \tag{77}$$

$$u_p = \sqrt{(P - P_1)(v_1 - v)}\,. \tag{78}$$

For the Tait equation of state over the range of interest in the present study ($P <$ 1 GPa), the U_s-u_p relationship is highly linear and the fitting coefficients are a_o = 1484 m/s and s = 1.974. This is consistent with the evaluation of Nagayama et al. (2002) who also show that the irreversible temperature rise is on the order of 10°C at 1 GPa so that the Hugoniot can be reasonably approximated by the isentrope as we have done using the Tait equation.

References

M. Arienti, P. Hung, E. Morano, and J. E. Shepherd. A level set approach to Eulerian-Lagrangian coupling. *J. Computational Physics*, 185:213–251, 2003.

R. M. Beam. Finite amplitude waves in fluid-filled elastic tubes: Wave distortion, shock waves, and korotkoff sounds. Technical Report TN D-4803, NASA, 1968.

W. M. Beltman and J.E. Shepherd. Linear elastic response of tubes to internal detonation loading. *Journal of Sound and Vibration*, 252(4):617–655, 2002.

W. M. Beltman, E. Burcsu, J.E. Shepherd, and L. Zuhal. The structural response of cylindrical shells to internal shock loading. *Journal of Pressure Vessel Technology*, pages 315–322, 1999.

R. A. Benham and T.A. Duffey. Experimental-theoretical correlation on the containment of explosions in cylindrical vessels. *Int. J. Mech. Sci.*, 16:549–558, 1974.

P.G. Bhuta. Transient response of a thin elastic cylindrical shell to a moving shock wave. *J. Acoustical Soc. America*, 35(1):25–30, 1963.

P. Chambers, H. Sandusky, F. Zerilli, K. Rye, R. Tussing, and J. Forbes. Pressure measurements on a deforming surface in response to an underwater explosion in a water-filled aluminum tube. *Shock and Vibration*, 8:1–7, 2001.

T. W. Chao. *Gaseous detonation-driven fracture of tubes*. PhD thesis, California Institute of Technology, 2004.

T. W. Chao and J. E. Shepherd. Comparison of fracture response of preflawed tubes under internal static and detonation loading. *Journal of Pressure Vessel Technology*, 126(3):345–353, August 2004.

T. W. Chao and J. E. Shepherd. Fracture response of externally flawed aluminum cylindrical shells under internal gaseous detonation loading. *International Journal of Fracture*, 134(1):59–90, July 2005a.

T. W. Chao and J.E. Shepherd. Detonation loading of tubes in the modified shear wave regime. In Z. Jiang, editor, *Proceedings of the 24th International Symposium on Shock Waves*, volume 2, pages 865–870. Springer, 2005b.

D. Coker and A. J. Rosakis. Experimental observations of intersonic crack growth in asymmetrically loaded unidirectional composite plates. *Philosophical Magazine A-Physics of Condensed Matter Structure Defects And Mechanical Properties*, 81:571–595, 2001.

R.H. Cole. *Underwater Explosions*. Dover, New York, NY, 1965.

VA Del Grosso. Analysis of multimodel acoustic propagation in liquid cylinders with realistic boundary conditions - application to sound speed and absorption measurements. *Acustica*, 24(6):299–311, 1971.

V. S. Deshpande, A. Heaver, and N. A. Fleck. An underwater shock simulator. *Proc. R. Soc. A*, 462:1021–1041, 2006.

T.A. Duffey. Approximate solutions of an impulsively loaded long cylinder governed by an elastic-plastic material law. *Acta Mechanica.*, 11:45–57, 1971.

T.A. Duffey and R. Krieg. Effects of strain hardening and strain rate sensitivity on the transient response of elastic-plastic rings and cylinders. *Int. J. Mech. Sci.*, 11: 825–844, 1969.

T.A. Duffey and D. Mitchell. Containment of explosions in cylindrical shells. *Int. J. Mech. Sci.*, 15:237–249, 1973.

T.A. Duffey, E.A. Rodriguez, and C. Romero. Design of pressure vessels for high-strain rate loading: dynamic pressure and failure criteria. Bulletin 477, Welding Research Council, P.O. Box 1942, New York, NY, 2002.

H.D. Espinosa, S. Lee, and N. Moldovan. A novel fluid structure interaction experiment to investigate deformation of structural elements subjected to impulsive loading. *Experimental Mechanics*, 46:805824, 2006.

F. Fanous and L. Greiman. Simplified analysis for impulsively loaded shells. *Journal of Structural Engineering*, 114:885–899, April 1988.

J. R. Florek and H. Benaroya. Pulse-pressure loading effects on aviation and general engineering structures. *Journal of Sound and Vibration*, 284:421–453, 2005.

G. R. Fowles. Attenuation of a shock wave produced in a solid by a flying plate. *J. Appl. Physics*, 31(655-661), 1960.

C. R. Fuller and F. J. Fahy. Characteristics of wave propagation and energy distributions in cylindrical elastic shells filled with fluid. *J. Sound Vibration*, pages 501–518, 1982.

J Gale and I Tiselj. Godunov's method for simulations of fluid-structure interaction in piping systems. 130(3):031304, 2008.

R. P. Greenwood. German work on grp design. *Composites*, 7:175–184, 1977.

J.B. Grotberg and O. E. Jensen. Biofluid mechanics in flexible tubes. *Annual Reviews of Fluid Mechanics*, 36:121–147, 2004.

P. G. Hodge. The influence of blast characteristics on final deformation of circular cylindrical shells. *Journal of Applied Mechanics*, 284:617–624, December 1956.

M. S. Howe. *Acoustics of Fluid-Structure Interaction*. Cambridge University Press, 1998.

D. Hull and T. W. Clyne. *An Introduction to Composite Materials*. Cambridge University Press, 2nd edition, 1996.

K. Inaba and J. E. Shepherd. Flexural waves in fluid-filled tubes subject to axial impact. In *Proceedings of the ASME Pressure Vessels and Piping Conference. July 27-31, Chicago, IL USA*, 2008a. PVP2008-61672.

K. Inaba and J. E. Shepherd. Impact generated stress waves and coupled fluid-structure responses. In *Proceedings of the SEM XI International Congress & Exposition on Experimental and Applied Mechanics. June 2-5, Orlando, FL USA*, 2008b. Paper 136.

N. Joukowsky. Über den hydraulischen stoss in wasserleitungsrohren. *Memoires de lAacademie Imperiale des Sciences de St. Petersbourg*, 1900. series 8, 9.

M. C. Junger and D. Feit. *Sound, Structures, and Their Interaction*. MIT Press, 1986.

V.K. Kedrinsky. *Hydrodynamics of Explosion*. Springer, 2005.

J. T. Kenney. Steady state vibrations of beam on elastic foundation for moving load. *J. Applied Mechanics. Trans. ASME*, 21(4):359–364, 1954.

H. Kolsky. *Stress Waves in Solids*. Dover Publications, Inc., 1963.

D. Korteweg. Über die fortphlanzungsgeschwindigkeit des schalles in elastisches rohren. *Annalen der Physik und Chemie, 9 floge*, 5:525–542, 1878.

O.E. Kosing and B. W. Skews. An investigation of high speed forming of circular plates in a liquid shock tube. *Int. J. Impact Engng*, 21(9):80181, 1998.

LD Lafleur and FD Shields. Low-frequency propagation modes in a liquid-filled elastic tube waveguide. *J. Acoust. Soc. Am.*, 97(3):1435–1445, 1995.

K. B. Lewis and N. V. Nechitailo. Transient resonance in hypervelocity launchers at critical velocities. *IEEE Transactions on Electromagnetics*, 43:157–162, 2007.

QS Li, K Yang, and L Zhang. Analytical solution for fluid-structure interaction in liquid-filled pipes subjected to impact-induced water hammer. *Journal of Engineering Mechanics*, 129(12):1408–1417, 2003.

Z. Liang, J. Karnesky, and J. E. Shepherd. Structural response to reflected detonations and deflagration-to-detonation transition in H_2-N_2O mixtures. Technical Report FM2006.003, California Institute of Technology, 2006a. Revised May 23, 2007.

Z. Liang, J. Karnesky, J.E. Shepherd, and R. Deiterding. Experimental measurements and numerical validation of reflected detonations in C_2H_4-O_2 mixtures. Technical Report FM2006.009, Graduate Aeronautical Laboratories, California Insititute of Technology, 2006b.

J. Lighthill. *Waves in Fluids*. Cambridge University Press, 1978.

S. P. Marsh, editor. *LASL shock hugoniot data*. University of California Press, Berkeley, CA, 1980.

M. A. Meyers. *Dynamic behavior of materials*. John Wiley & Sons, 1994.

K. Nagayama, Y. Mori, K. Shimada, and M. Nakahara. Shock hugoniot compression curve for water up to 1 GPa by using a compressed gas gun. *Journal of Applied Physics*, 91(1), 2002.

ONR. Underwater explosion research: A compendium of the British and American reports, Vol. I The shock wave, Vol. II-The gas globe, Vol. III-The damage process. Technical report, Office of Naval Research, Washington, DC., 1950.

KH Parker. A brief history of arterial wave mechanics. *Med. Biol. Eng. Comput.*, 47(2):111–118, 2009.

R. J. Pinnington. The axisymmetric wave transmission properties of pressurized flexible tubes. *Journal of Sound and Vibration*, 204:271–289, 1997.

F. Pintgen and J. E. Shepherd. Elastic and plastic structural response of thin tubes to deflagration-to-detonation transition events. Technical Report FM2005.008, California Institute of Technology, March 2006.

R. Rajendran and K. Narasimhan. Deformation and fracture behaviour of plate specimens subjected to underwater explosion - a review. *International Journal of Impact Engineering*, 32:1945–1963, 2006.

E.A. Rodriguez and T.A. Duffey. Fracture-safe and fatigue design criteria for detonation-induced pressure loading in containment vessels. Bulletin 494, Welding Research Council, P.O. Box 1942, New York, NY, 2004.

H. Sandusky, P. Chambers, F. Zerilli, L. Fabini, and W. Gottwald. Dynamic measurements of plastic deformation in a water-filled aluminum tube in response to detonation of a small explosive charge. *Shock and Vibration*, 6:125–132, 1999.

J. E. Shepherd. Structural response of piping to internal gas detonation. *Journal of Pressure Vessel Technology*, 2009. in press.

J.E. Shepherd, J. Karnesky, F. Pintgen, and J. C. Krok. Experimental measurements of strains and blast waves resulting from detonations in tubes. Technical Report FM2006.010, Graduate Aeronautical Laboratories, California Insititute of Technology, June 2008.

T. E. Simkins. The influence of transient flexural waves on dynamic strains in cylinders. *J. Applied Mechanics*, 62:262–265, 1995.

T. E. Simkins, G. A. Pflegl, and E. G. Stilson. Dynamic strains in a 60-mm gun tube: An experimental study. *J. Sound Vibration*, 168:549–557, 1993.

B. K. Sinha, T. J. Plona, S. Kostek, and S.-K. Chang. Axisymmetric wave propagation in fluid-loaded cylindrical shells. *J. Acoust. Soc. Am.*, 132(2):1132–1143, August 1992.

R. Skalak. An extension to the theory of water hammer. *Transactions of the ASME*, 78:105–116, January 1956.

B.W. Skews, E. Kosing, and R.J. Hattingh. Use of a liquid shock tube as a device for the study of material deformation under impulsive loading conditions. *Proc. Instn. Mech. Engrs. J. Mechanical Engineering Science*, 218:39–51, 2004.

W. R. Smith. Fast loading of metals with a shock tube: Application to aluminum. In *Proceedings of the 15th International Symposium on Shock Waves, Berkeley CA 1985*, pages 541–545. Stanford University Press, 1986.

W. R. Smith. Modeling inelastic wall response of a thin-walled cylindrical tube to shock waves. In *Proceedings of the 17th International Symposium on Shock Waves, Bethlehem PA 1989*, pages 558–563, New York, NY, 1990. American Institute of Physics.

B. Spencer and D. Hull. Effect of winding angle on the failure of filament wound pipe. *Composites*, 9:263–271, 1978.

S. Tang. Dynamic response of a tube under moving pressure. In *Proceedings of the American Society of Civil Engineers*, volume 5, pages 97–122. Engineering Mechanics Division, October 1965.

A. S. Tijsseling. Fluid-structure interaction in liquid-filled pipe systems: a review. *Journal of Fluids and Structures*, 10:109–146, 1996.

A. S. Tijsseling. Exact solution of linear hyperbolic four-equation system in axial liquid-pipe vibration. *Jourbal of Fluids and Structures*, 18:179–196, 2003.

A. S. Tijsseling. Water hammer with fluid-structure interaction in thick-walled pipes. *Computers and Structures*, 85:844–851, 2007.

A. S. Tijsseling, M. F. Lambert, A. R. Simpson, M. L. Stephens, John P. Vitkovsky, and A. Bergant. Skalak's extended theory of water hammer. *J. Sound Vibration*, 310:718–728, 2008.

D.H. Trevena. *Cavitation and Tension in Liquids*. Adam Hilger, 1987.

A. B. Wardlaw, Jr. and J. Alan Luton. Fluid structure interaction mechanisms for close-in explosions. *Shock and Vibration*, 7:265–275, 2000.

G. Z. Watters. *Analysis and Control of Unsteady Flow in Pipelines*. Butterworth Publishers, MA, 1984.

DC Wiggert and AS Tijsseling. Fluid transients and fluid-structure interaction in flexible liquid-filled piping. *Applied Mechanics Reviews*, 54(5):455–481, 2001.

DC Wiggert, FJ Hatfield, and S Stuckenbruck. Analysis of liquid and structural transients by the method of characteristics. *J. Fluids Eng.*, 109(2):161–165, 1987.

E. B. Wylie and V. L. Streeter. *Fluid Transients in Systems*. Prentice-Hall, Inc., NJ, 1993.

Z. Xue and J. W. Hutchinson. A comparative study of impulse-resistant metal sandwich plates. *International Journal of Impact Engineering*, 30:1283–1305, 2004.